Gamma Ray Burst Afterglows: A Theoretical Exploration

Mehul Goyal (22B1809)
Under the guidance of Prof. Varun Bhalerao
Department of Physics
Indian Institute of Technology Bombay

Contents

Abstract

Gamma-Ray Bursts (GRBs) are among the most energetic phenomena in the universe, characterized by intense gamma-ray emission followed by long-lived afterglows across the electromagnetic spectrum. This project presents a comprehensive theoretical and observational study of GRB afterglows, focusing on the physical mechanisms governing their temporal evolution. Beginning with relativistic hydrodynamics and synchrotron radiation theory, we derive scaling relations that describe afterglow fading in different environments—constant-density interstellar media (ISM), stratified wind-like profiles, and under conditions of continued energy injection from the central engine. We further explore geometric effects such as jet collimation. These theoretical predictions are applied to multiband observational data from GRB230204B. Using Bayesian inference with the dynesty nested sampler, we fit a wind-medium model to the light curves and recover physical parameters consistent with a low-efficiency GRB and $p \sim 2.76$ electron distribution index. The model successfully reproduces key features, including the theoretically predicted constant flux in late-time radio observations. This work shows how broadband afterglow modelling can yield insights into GRB progenitors, jet energetics, and circumburst environments, and lays the groundwork for future bulk-analysis GRBs in the GROWTH-India catalogue.

1 Overview

1 What are Gamma Ray Bursts ?

Gamma Ray Bursts (GRBs) are the brightest and the most luminous explosions in the Universe, emitting intense flashes of gamma rays (Piran, 2004). For their duration, they can outshine their entire host galaxies (Kumar & Zhang, 2015). They were first detected by the Vela Satellites launched in the 1960s to monitor nuclear activity (Klebesadel et al., 1973). However, their extragalactic origins were confirmed much later (Metzger et al., 1997). Their isotropic distribution in the sky and vast luminosities fueled the initial scepticism towards extragalactic origins (Fishman & Meegan, 1995), and the discovery of afterglows in 1997 and subsequent redshift measurements confirmed it (van Paradijs et al., 1997).

The duration of a GRB is measured by their T90 value, which is the duration in which 5% and 95% of the total energy of the burst is emitted (Kouveliotou et al., 1993). Observationally, we find a bimodal distribution (Nakar, 2007). Long GRBs, lasting more than 2 seconds, are typically associated with the collapse of massive stars (hypernovae; Woosley & Bloom, 2006). In contrast, short GRBs, lasting less than 2 seconds, are believed to result from the mergers of compact objects such as neutron stars (Berger, 2014). Short GRBs tend to be harder than Long GRBs, where *hardness* is the ratio of the number of photons in the high-energy channel to the number of photons in the low-energy channel (Gehrels et al., 2009).

Gamma-ray bursts are powered by narrow, ultra-relativistic jets driven by the central engine. These jets travel into the surrounding medium at ultrarelativistic speeds. The interaction of the jet with the external surrounding medium produces afterglow emission, and the internal dissipation of the jet is the source of prompt emission. The radiation we detect from the jets is highly beamed in the direction of motion of the jet due to *relativistic beaming*. Hence, the emission can only be observed if we lie on the *line of sight* of the jet. This leads to interesting phenomena like *orphan afterglows*, where we entirely miss the initial prompt emission, and only observe the late-time afterglow emission, when the jet has slowed and expanded sideways enough for us to lie in the line of sight. Figure 1.1 presents an illustration of what a Gamma-ray burst mechanism looks like. We can see a jet cruising into the external medium. The sites of afterglow and prompt emission have also been marked.

2 What are GRB Afterglows ?

The afterglow arises from the interaction of relativistic ejecta with the circumburst medium (Piran, 2004). As the shockwave produced by the burst propagates outwards and decelerates, it accelerates the charged particles in the surrounding medium, causing them to emit radiation, primarily through the synchrotron process (Meszaros, 2006). The afterglow emission is broadband emission; hence, it is detected across the electromagnetic spectrum, from x-rays to radio (van Paradijs et al., 1997). The behavior of afterglow across different frequencies can be modelled using shock physics and the synchrotron emission theory, with the key frequencies (e.g. characteristic, peak and cooling) playing an essential role in determining the spectral and temporal properties of the afterglow

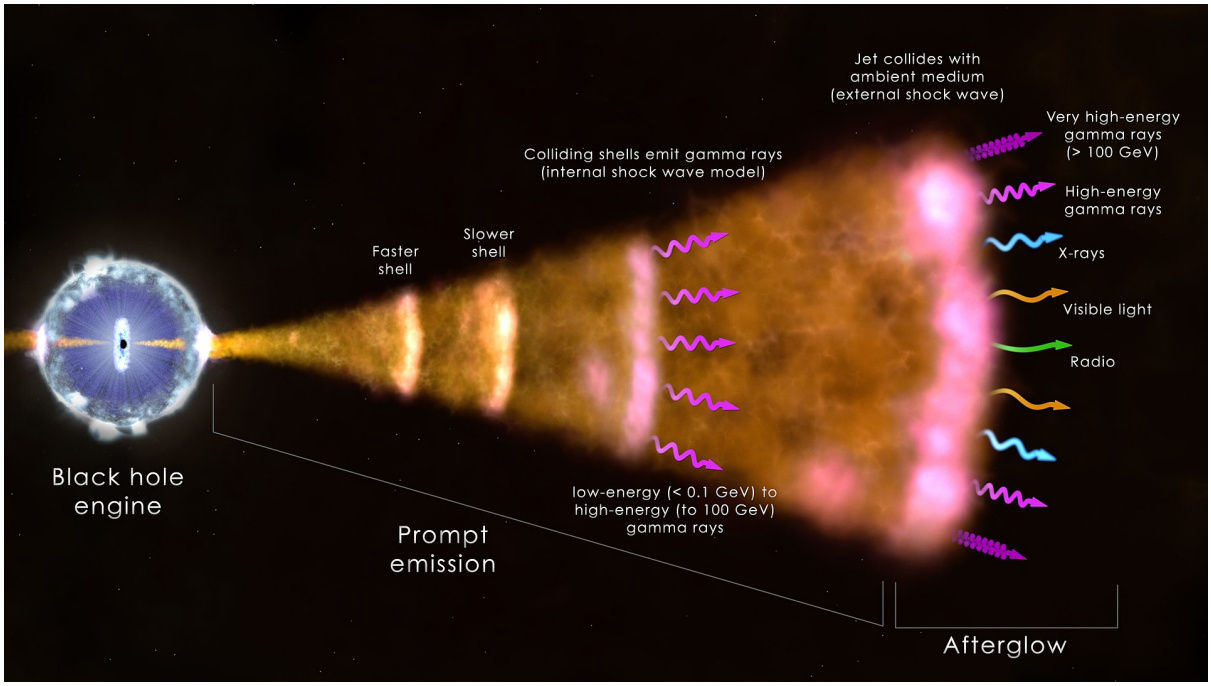

Figure 1.1: GRB Mechanism (Credit: NASA/Goddard Space Flight Center/ICRAR)

emission (Sari et al., 1998).

2.1 Significance of Studying GRB Afterglows

Afterglow observations are key to probing the underlying physics of Gamma-Ray Bursts (GRBs) beyond the prompt emission. They offer valuable insights into the energy distribution and geometry of relativistic jets, the density structure and composition of the circumburst medium, and the nature of the central engine (Kumar & Zhang, 2015). Optical observations from the afterglow allow measurement of the GRB's redshift as well. Broadband data helps us identify host galaxies and help characterise the surrounding environment (Metzger et al., 1997).

In particular, the *fading behaviour* of GRB afterglows encodes a lot of information about the post-explosion evolution. The GRB flux fades as the shockwave slows down due to interaction with the surrounding medium and increasing accumulated mass. The temporal decay of observed flux can be used to constrain the emission mechanisms, properties of the surrounding medium, jet structure, and even the activity of the central engine at late times.

In this project, I focus on studying the fading of GRB afterglows and the various physical factors that govern their evolution. A schematic comparing different fading phases is shown in Figure 1.2. .

3 Factors influencing Fading of GRB Afterglows

In this project, I focused on studying the fading of GRB Afterglows and different physical factors which influence the fading of an afterglow.

The fading of afterglow flux is primarily influenced by and provides insights in

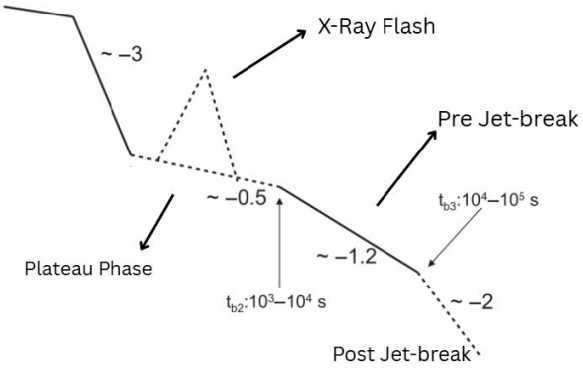

Figure 1.2: Figure comparing fading of afterglows in different phases. The diagram purposely has no axes drawn, as it only serves the purpose of comparing slopes in different phases. The y-axis is Flux and x-axis is time.

- **Emission Mechanisms**: There can be many emission mechanisms fuelling the afterglow emission. The charged particles in post-shock plasma, under the influence of the power magnetic fields of the central engine, emit synchrotron radiation. Synchrotron radiation is the primary emission mechanism in afterglow emission. The charged particles can also undergo inverse Compton scattering. In both, it is primarily electrons that emit the radiation because they are 2000 times lighter than protons.

- **Environment Density Profile**: GRBs are formed by the core collapse of very massive stars. Stars can influence the interstellar medium surrounding them through powerful stellar winds. These winds can change the density profile of the surrounding medium. Different types of stars can give rise to different density profiles. The density profile influences how fast the afterglow fades, as we will see in upcoming sections.

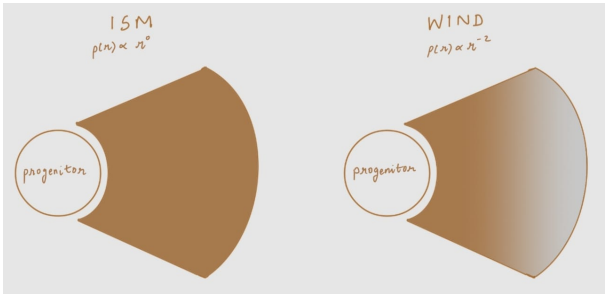

Figure 1.3: Depiction of ISM and Wind-type medium

- **Central Engine Behavior**: One of the widely accepted models of Gamma Ray Bursts is the Fireball model. The fireball model assumes that the central engine emits all the energy of the gamma-ray burst initially and goes quiet afterwards. However, in reality, this may not be the case. The central engine can show periods of late time activity in the form of stable continuous energy injection or in the form of short, powerful flares. Such central engine activity can cause the afterglow light curve to deviate from what we would ideally obtain from synchrotron emission. This can explain the plateau phases in some GRB afterglows.

- **Jet Structure**: Generally, we assume that the energy of the jet is independent of the angle within the jet. This is called the top-hat jet model. However, it can be the case that energy is a function of $\theta < \theta_{\text{jet}}$. The energy can be a falling power law or even a gaussian.

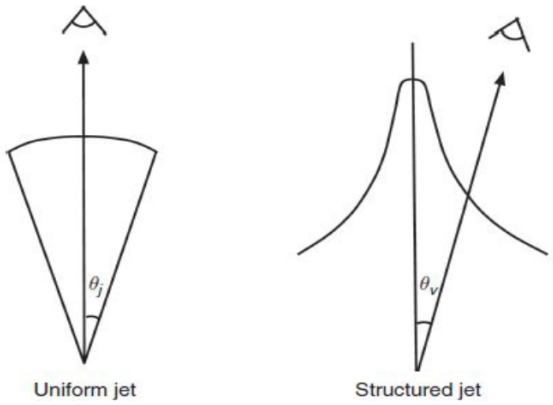

Figure 1.4: Uniform Jet (left) and Structured Jet (right) (Zhang, 2018)

- **Observing Angle**: The observer's viewing angle may not always align with the jet of the GRB. The resultant flux varies for different viewing angles. In case of *highly relativistic* outflow, the emission from the jet is highly concentrated within a cone of angle $\theta_{\text{beam}} \sim \frac{1}{\Gamma}$. If the observer angle is greater than the beaming angle, but smaller than the jet opening angle ($\theta_{\text{jet}} > \theta_{\text{view}} > \theta_{\text{beam}}$), then we see a shallower decay than expected because, as the gamma of the jet reduces, more and more emitting material comes in the view of the observer.

2 Theoretical Foundations

In this chapter, we will cover the theoretical foundations necessary to discuss and derive the temporal evolution of afterglows. First, we will delve into relativistic hydrodynamics and derive the shock conditions at the shock discontinuity. We will then study the shocks in the *strong shock condition*. In the next section, we will discuss *Synchrotron radiation*. We will start with a discussion of the spectrum of a single electron and then from a population of electrons. Finally, we will discuss different *frames* involved in the problem and relate the time-scales in these frames.

1 Relativistic Hydrodynamics

The macroscopic behaviour of fluids can be derived from the microscopic physics of the particles using the Kinetic Theory of Fluids. In this approach, instead of solving the Newtonian Equations of Motion for each fluid particle, we describe the system using a distribution function defined over the phase space. The distribution function captures the number density of particles over position and momentum. Using the distribution function, we can calculate the macroscopic observable properties like density, temperature and pressure. This section is inspired by chapter 8 of (Padmanabhan, 2000).

1.1 What is Distribution Function?

The distribution function is defined as follows

$$dN = f(x, p, t) d^3x d^p, \tag{2.1}$$

where $f(x, p, t)$ is the distribution function, dN is the number of particles in the phase space volume element, and $dV_p = d^3x d^3p$ is the phase space volume element.

The distribution function can change from the following two processes:

- Macroscopic Force Fields
- Collisions or interactions generated from short-ranged intermolecular forces

The collisions between the fluid elements will change the distribution function of the fluid. A differential change in the distribution function is

$$df = \frac{\partial f}{\partial t} + \sum_i \frac{\partial x_i}{\partial t}\frac{\partial f}{\partial x_i} + \sum_i \frac{\partial v_i}{\partial t}\frac{\partial f}{\partial v_i} = C[f]$$

where

- **i** is the index which runs over a number of particles
- $C[f]$ is the collision term

This is the *Boltzmann Equation* and governs the evolution of the distribution function in the phase space.

We can define several physical quantities of the system (Current Density four-vector and Stress Energy Tensor) by taking *moments* of the distribution of the function. In the following section, I take the moments of the distribution function and interpret the various components of these tensors.

1.2 Moments of Distribution Function

Taking the first moment, we can define the following four-vector

$$J^{\alpha}(x^i) = c \int \frac{d^3\vec{p}}{E_p} p^{\alpha} f(x^i, \vec{p}) \tag{2.2}$$

Here, p^{α} is the momentum four-vector.

$$p^{\alpha} = \left(\frac{E_p}{c}, \gamma m_0 v_x, \gamma m_0 v_x, \gamma m_0 v_y, \gamma m_0 v_z \right) \tag{2.3}$$

We can interpret the components of this four-vector as follows:

$$J^0(x^i) = \int d^3\vec{p} f(x^i, p) = n(x^i), \tag{2.4}$$

which is the number of particles in a unit spatial volume. The spatial components of the four-vector are

$$\vec{J}(x^i) = \frac{1}{c} \int d^3\vec{p} f(x^i, p) \vec{v} = \frac{1}{c} n(x^i) \langle v \rangle \tag{2.5}$$

which is the flux of particles in each spatial direction, and $\langle v \rangle$ is the flow velocity in bulk at the given spatial location.

Similarly, we can write the quadratic moments.

$$T^{\alpha\beta}(x^i) = c^2 \int \frac{d^3\vec{p}}{E_p} p^{\alpha} p^{\beta} f(x^i, \vec{p}) \tag{2.6}$$

$T^{\alpha\beta}$ is the energy-momentum tensor of the system. The components of this rank-2 tensor can be interpreted as follows.

$$T^{00} = \int d^3\vec{p} E_p f(x^i, \vec{p}) \tag{2.7}$$

Here, $T^{00}(\vec{x})$ gives the energy density of the system.

$$T^{0i} = T^{i0} = c \int d^3\vec{p} p^i f(x^i, \vec{p}) \tag{2.8}$$

$T^{0i}(\vec{x})$ gives the density of i^{th} component of spatial momentum.

$$T^{ij} = T^{ji} = \int d^3\vec{p} p^i v^j f(x^i, \vec{p}) \tag{2.9}$$

T^{ij} gives the i^{th} component of spatial momentum that crosses the unit area orthogonal to j^{th} direction per unit of time.

In an upcoming section, we will derive the conservation laws (mass, momentum and energy) for the system using the above-defined quantities.

Here, I would like to highlight an important assumption in all upcoming discussions. We assume that the collisions between the fluid elements are of such a nature that the respective quantities are conserved in each collision. The collisions in which mass, momentum and energy of particles are conserved are termed as *elastic collisions*. Hence, we limit our discussion to fluids with elastic collisions.

In the absence of external forces, the conservation laws for a fluid with elastic collisions are reduced to

$$\frac{\partial J^{\alpha}}{\partial x^{\alpha}} = 0 \ , \frac{\partial T^{\alpha\beta}}{\partial x^{\alpha}} = 0 \tag{2.10}$$

1.3 Stress Energy Tensor of an Ideal Fluid

We want to construct a rank-2 tensor that encodes the energy-momentum content of the fluid system and is constructed from the known fluid quantities. We also require the tensor to be symmetric.

The most general form *symmetric*, *second rank tensor* which can be constructed from the above quantities is

$$T^{\mu\nu} = Au^\mu u^\nu + B\eta^{\mu\nu} \tag{2.11}$$

The above equation is a tensor equation, which respects Lorentz transformations; hence, the equation is frame-invariant. Solving the equation in rest frame of the fluid, we get

$$T^{00} = \rho c^2 + e \tag{2.12}$$

$$T^{ij} = P\delta^{ij} \tag{2.13}$$

$$T^{0i} = 0 \tag{2.14}$$

From the above, we get the following three conditions

$$A - B = \rho c^2 + e \qquad \text{Equation 2.12} \tag{2.15}$$

$$B = P \qquad \text{Equation 2.13} \tag{2.16}$$

$$\text{The third equation is trivially true!} \qquad \text{Equation 2.14} \tag{2.17}$$

From the above we get, $A = \rho c^2 + e + P$ and $B = P$. Therefore, the relativistic stress-energy tensor of an ideal fluid is

$$T^{\mu\nu} = \left(\rho c^2 + e + P\right) u^\mu u^\nu + P\eta^{\mu\nu} \tag{2.18}$$

The interpretation of J^α is straightforward. It is the current density. Hence $J^\alpha = \rho u^\alpha$, where u^α is the normalized 4-velocity

1.4 Conservation Laws for a relativistic ideal fluid

Let the four-dimensional event vector be $x^\mu = (ct, \vec{x})$ and proper time $d\tau = \frac{dt}{\gamma}$. Then, the normalized 4-velocity is

$$u^\mu = \frac{dx^\mu}{d\tau} = \gamma\left(1, \frac{\vec{v}}{c}\right)$$

For ease of calculation, I will work in natural units, in which the value of reduced Plank's constant and speed of light is 1; $\hbar = 1, c = 1$. Also, I use the notation, $\partial_\mu \equiv \frac{\partial}{\partial x^\mu}$.

The Mass Conservation equation is

$$\frac{\partial J^\mu}{\partial x^\mu} = \partial_\mu(\rho u^\mu) = \frac{\partial(\gamma\rho)}{\partial t} + \vec{\nabla}\cdot(\gamma\rho\vec{v}) = 0 \implies \text{Continuity Equation} \tag{2.19}$$

The energy-momentum conservation is encoded in $\frac{\partial T^{\mu\nu}}{\partial x^\mu} = 0$ The energy conservation equation is obtained by setting $\nu = 0$. I use $h = \rho c^2 + e + P$, which is the enthalpy density of the fluid.

$$\partial_\mu T^{\mu 0} = \partial_m u\left[\gamma\left(\rho + e + P\right)u^\mu + P\eta^{\mu 0}\right] \tag{2.20}$$

$$= \partial_\mu\left[\gamma h\mu + \rho\eta^{\mu 0}\right] \tag{2.21}$$

$$= \partial_\mu\left(\gamma h u^\mu\right) - \frac{\partial P}{\partial t} \tag{2.22}$$

$$= \frac{\partial(\gamma^2 h)}{\partial t} - \frac{\partial P}{\partial t} + \vec{\nabla}\cdot(\gamma^2 h\vec{v}) = 0 \implies \text{Energy Conservation} \tag{2.23}$$

The conservation of momentum equation can be obtained setting $\nu = i$.

$$\partial_\mu T^{\mu i} = \partial_\mu \left[\gamma h u^\mu u^i + P\eta^{\mu i}\right] \tag{2.24}$$

$$= \gamma h u^\mu \partial_\mu u^i + u^i \partial_m u(\gamma h u^i) + \eta^{\mu i}\partial_\mu P \tag{2.25}$$

$$= \vec{v}\frac{\partial(\gamma^2 h)}{\partial t} + \vec{\nabla}\cdot(\gamma^2 h\vec{v})\vec{v} + \vec{\nabla}P + \gamma^2 h\left[\frac{\partial}{\partial t} + \vec{v}\cdot\vec{\nabla}\right]\vec{v} \tag{2.26}$$

$$= \vec{v}\frac{\partial(\gamma^2 h)}{\partial t} + \left[\frac{\partial P}{\partial t} - \frac{\partial(\gamma^2 h)}{\partial t}\right]\vec{v} + \vec{\nabla}P + \gamma^2 h\frac{\partial\vec{v}}{\partial t} + \gamma^2 h(\vec{v}\cdot\vec{\nabla})\vec{v} \tag{2.27}$$

$$= \gamma^2 h\frac{\partial\vec{v}}{\partial t} + \gamma^2 h(\vec{v}\cdot\vec{\nabla})\vec{v} + \vec{v}\frac{\partial P}{\partial t} + \vec{\nabla}P = 0 \implies \text{Energy Conservation} \tag{2.28}$$

In all the above equations, c can be introduced everywhere necessary by dimensional analysis. I choose not to do that right now, as it is unnecessary.

2 Shocks in Hydrodynamics

Having covered the fundamentals of hydrodynamics in the above sections, we can now discuss shocks in fluids. Shocks arise naturally in almost all astrophysical scenarios. Hence, it is of utmost importance to address the theoretical foundations of shocks in relativistic fluids.

In this section, I will first start by discussing what shocks are, introduce the basic terminology, and then we will proceed to derive the relativistic Rankine-Hugionot conditions, i.e. the jump conditions at the shock discontinuity. For this section, I refer to Modern Classical Physics by (Thorne & Blandford, 2018), and Volume 6 of (Landau & Lifshitz, 1987)

2.1 Introduction

A shock front occurs in a fluid when the velocity gradient in that region becomes very large or diverges. Other terms commonly used for a shock front include "shock waves" or simply "shocks". Within the shock region, we can no longer disregard the viscous stress. However, the scales of the problem allow us to proceed without referring to viscous processes in the internal structure of the shock, as we will discuss in the following subsection.

Now, I will introduce the basic terminology we will use throughout this section. The *upstream* of the shock refers to the cool *supersonic* fluid ahead of the shock, while the *downstream* is the hot subsonic flow that follows the shock front.

Shock Front is a discontinuity in fluid

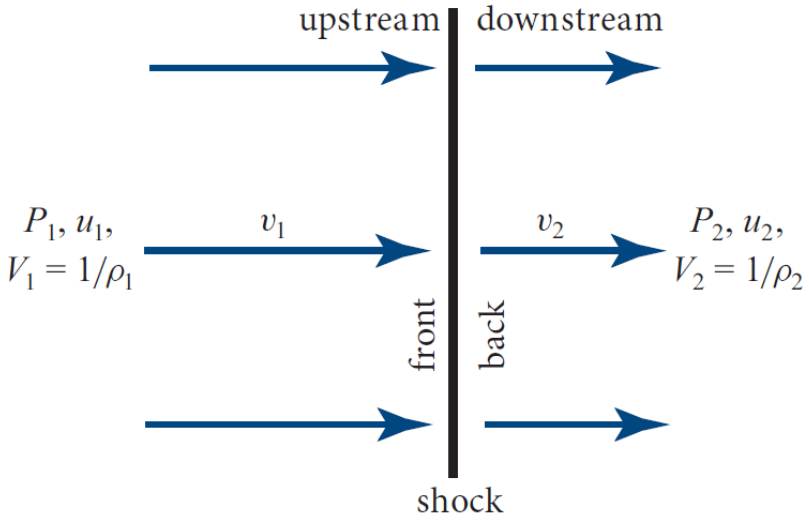

Figure 2.1: Shock front

In astrophysics, the length scales of the upstream and downstream regions of a flow are typically much larger than the scale of the shock, which is the area where a large velocity gradient occurs. As a result, the timescales in the upstream and downstream flows are significantly longer than the time it takes for the fluid to cross the shock region.

This allows us to deduce the behaviour of the fluid without needing to reference the detailed structure of the shock. Instead, we can focus on the appropriate conditions for the upstream and downstream flows in terms of conservation laws. While viscosity is crucial within the shock region, we can analyze the upstream and downstream flows without delving into the specifics of viscous processes. We conduct the analysis in the rest frame of the shock, in which the upstream particles flow into the shock front at relativistic speeds.

2.2 Conservation across the Shock Front

I will start this section by introducing the notation used by Thorne & Blandford (2018) in his book.

$$[F] = F_1 - F_2$$

where F_1 refers to the value of the function in the upstream region and F_2 refers to the value of the function in the downstream region.

Using the above notation, mass, momentum and energy conservation equations across the shock for stationary flow can be written as follows. In simplest terms, stationary flow is time-independent flow, by which I mean $\frac{\partial(\text{Everything})}{\partial t} = 0$. However, note that this does not imply that flow is uniform. You may recognise stationary flow as steady flow, a more commonly used term.

- From Mass Conservation, we get

$$[\gamma\rho\vec{v}.\hat{n}] = 0 \implies \gamma_1\rho_1 v_1 = \gamma_2\rho_2 v_2$$

- From Energy Conservation:

$$[\gamma^2 hv] = 0 \implies \gamma_1^2 h_1 v_1 = \gamma_2^2 h_2 v_2$$

- from Momentum Conservation:

$$[\gamma^2 v^2 h] = 0 \implies \gamma_1^2 v_1^2 h_1 = \gamma_2^2 v_2^2 h_2$$

The above conditions are called *Rankine-Hugionot* conditions for a relativistic fluid.

2.3 Strong Shock and cold ISM Approximation

In Gamma Ray Bursts, we can make the following approximations (Zhang, 2018).

- The interstellar medium is *cold*. By this, we mean that internal energy (hereafter denoted by e) and pressure (P) are zero.
- The shock is *strong*. By this, I simply mean that the Lorentz factor of the shock is very large, i.e. $\Gamma \gg 1$ (And note, $\Gamma \sim \gamma_1$ since we are in the frame of the shock).

Under the above mentioned assumptions, by going through some tedious algebra, we can derive the following expression from the above three conditions.

$$\frac{e_2}{n_2} = \left(\frac{\gamma_1\gamma_2}{1-\beta_1\beta_2} - 1\right) m_p c^2$$

where

$$\beta_i = \frac{v_i}{c} \tag{2.29}$$

$$m_p = \text{mass of the proton} \tag{2.30}$$

$$\gamma_{21} = \frac{\gamma_1 \gamma_2}{1 - \beta_1 \beta_2} \tag{2.31}$$

and,

$$\frac{n_2}{n_1} = \frac{\hat{\gamma}\gamma_{21} - 1}{\hat{\gamma} - 1}$$

where

- $\hat{\gamma}$ is the adiabatic index of the medium and was used to relate pressure and density. In general, $\hat{\gamma}$ is defined as $\frac{\partial P}{\partial \rho} = \frac{\hat{\gamma} P}{\rho}$. In Gamma-ray bursts, in the frame of the shock, the upstream medium is moving at *ultra-relativistic speeds*; hence, the adiabatic index approaches that of photons, i.e. $\hat{\gamma} = \frac{4}{3}$

Now, we can manipulate the above expressions to derive the internal energy density of the downstream medium in terms of upstream quantities, primarily the Lorentz factor of the upstream medium.

$$e_2 = (\gamma_{21} - 1) n_2 m_p c^2$$

$$e_2 \simeq \gamma_{21} n_2 m_p c^2 \quad (\gamma_1 \gg 1 \implies \gamma_{21} \gg 1) \text{ check Equation 2.31}$$

$$e_2 \simeq 4\gamma_{21}^2 n_1 m_p c^2 \quad \left(\frac{n_2}{n_1} = \frac{\hat{\gamma}\gamma_{21} - 1}{\hat{\gamma} - 1} \text{ under ultra-relativistic limit implies } \frac{n_2}{n_1} \simeq 4\gamma_{21} \right)$$

The above equation is of crucial importance and will play an important role in the derivation of scaling relations for the temporal evolution of afterglows.

We pause our discussion of relativistic hydrodynamics and shocks here. We will return to it when we start deriving equations of the temporal evolution of afterglow after discussing other theoretical foundations. Now, we move to the primary emission mechanism in afterglows, i.e. the *Synchrotron Radiation*.

3 Synchrotron Radiation

For thoroughness, I will very briefly mention radiation fields for a charged particle and derive the power emitted by a relativistic particle under the influence of a magnetic field in the time domain. After that, we will delve into the synchrotron spectrum of a single charged particle and then derive the spectrum for a population of electrons. A significant part of the latter will discuss the case of GRBs, which has continuous injection of particles into the downstream region from the upstream ISM. This section refers to chapter 23 of Zangwill (2012), chapter 6 of Rybicki & Lightman (1979) and chapter 5 of Zhang (2018).

3.1 Synchrotron Power in Time domain

Liénard-Wiechert Potentials & Electromagnetic field

The electromagnetic fields produced by a moving point charge can be fully described using the Liénard-Wiechert potentials. For a point charge q moving along an arbitrary trajectory, the scalar and vector potentials at a field point $\mathbf{r}$ and time t are given by:

$$\phi(\mathbf{r},t) = \frac{q}{4\pi\epsilon_0}\frac{1}{(1-\mathbf{n}\cdot\beta)R}\bigg|_{\text{ret}}, \tag{2.32}$$

$$\mathbf{A}(\mathbf{r},t) = \frac{q\beta}{4\pi\epsilon_0 c}\frac{1}{(1-\mathbf{n}\cdot\beta)R}\bigg|_{\text{ret}} \tag{2.33}$$

,
where:

- $\beta = \mathbf{v}/c$ is the velocity of the charge normalized to the speed of light,
- $\mathbf{n}$ is the unit vector pointing from the source to the observer,
- R is the distance from the charge to the observer,
- All quantities are evaluated at the *retarded time* t_{ret}, defined implicitly by:

$$t_{\text{ret}} = t - \frac{R(t_{\text{ret}})}{c}.$$

From these potentials, the electric and magnetic fields can be derived using:

$$\mathbf{E} = -\nabla\phi - \frac{\partial\mathbf{A}}{\partial t}, \quad \mathbf{B} = \nabla\times\mathbf{A}.$$

The key physical insight is that the fields split into two parts: one that falls off as $1/R^2$, and one that falls off as $1/R$ (the radiation field). The radiation field arises purely from the acceleration of the charge and is responsible for the energy radiated to infinity.

One can do the algebra and verify that the radiation Electric and magnetic fields are

$$\mathbf{E} = \frac{q}{4\pi\epsilon_0}\left[\frac{(\hat{\mathbf{n}}-\beta)(1-\beta^2)}{g^3R^2} + \frac{\hat{\mathbf{n}}\times\left\{(\hat{\mathbf{n}}-\beta)\times\dot{\beta}\right\}}{cg^3R}\right]\bigg|_{\text{ret}} = \mathbf{E}_v + \mathbf{E}_a \tag{2.34}$$

$$\mathbf{B} = \frac{\mu_0 q}{4\pi}\left[\frac{(\mathbf{v}\times\hat{\mathbf{n}})(1-\beta^2)}{g^3R^2} + \frac{(\beta\times\hat{\mathbf{n}})(\dot{\beta}\cdot\hat{\mathbf{n}}) + g\,\dot{\beta}\times\hat{\mathbf{n}}}{g^3R}\right]\bigg|_{\text{ret}} = \mathbf{B}_v + \mathbf{B}_a \tag{2.35}$$

where:

- B_v and B_a are the velocity field and radiation field components of the magnetic field.
- E_v and E_a are the velocity field and radiation field components of the electric field.
- $g = (1-\beta.\hat{\mathbf{n}})$

Radiation Power

The power radiated at retarded time in a solid angle $d\Omega$ of a distant sphere of radius R is given by

$$dP = g_{\rm ret} R^2 \mathbf{S} \cdot \hat{\mathbf{n}} d\Omega$$

where $\mathbf{S}$ is the pointing vector.

For radiating fields, the Poynting vector is

$$\mathbf{S}(t) = \frac{1}{\mu_0}\mathbf{E}_a \times \mathbf{B}_a = \epsilon_0 c E_a^2 \, \hat{\mathbf{n}}_{\rm ret} = \epsilon_0 c \left(\frac{q}{4\pi\epsilon_0}\right)^2 \left| \left[\frac{\hat{\mathbf{n}} \times \left[(\hat{\mathbf{n}} - \beta) \times \dot{\beta}\right]}{c g^3 R} \right]_{\rm ret} \right|^2 \hat{\mathbf{n}}_{\rm ret}, \quad (2.36)$$

Replacing $\mathbf{S}$ in equation for Power, we get

$$\frac{dP}{d\Omega} = \frac{q^2}{16\pi^2\epsilon_0 c} \left| \left[\frac{\hat{\mathbf{n}} \times \left[(\hat{\mathbf{n}} - \beta) \times \dot{\beta}\right]}{c g^3 R} \right]_{\rm ret} \right|^2 \quad (2.37)$$

In synchrotron radiation, only the component perpendicular to the magnetic field accelerates. The magnetic field does not affect the component of velocity parallel to the magnetic field and, hence, does not contribute to it. The component of velocity, perpendicular to a magnetic field, undergoes circular motion.

Integrating the above over all angles, we can derive Larmor's formula in the relativistic case in which velocity is perpendicular to the acceleration. Here I have taken the ultrarelativistic limit ($\gamma \gg 1$ and $\theta \to 0$) and eliminated θ dependence by setting $\theta = 0$ in the ultrarelativistic limit. I do not care about θ dependence as it has no effect on scaling relations for the temporal evolution of afterglows we derive later (θ dependence can be included; it's only algebra). This expression is important because in the next section, we take the Fourier transformation of this to find the power spectrum.

$$P = \frac{2q^2}{3c^3}\gamma^2 \frac{q^2 B^2}{m^2}\beta_\perp^2$$

3.2 Synchrotron Spectrum from a Single Electron

Synchrotron Spectrum is Broadband

.We consider a single electron of energy $E = \gamma m_e c^2$ spiralling in a uniform magnetic field $\mathbf{B}$ at a pitch angle α (the angle between velocity and magnetic field). Because of relativistic beaming, to a distant observer, the radiation seems to be confined to a narrow cone (refer to the figure below). Hence, the observer sees a pulse of radiation for a very small time interval compared to the rotation time period of the electron. Precisely due to this, the synchrotron spectrum will be broadband. I refer to Rybicki and Lightman for this derivation.

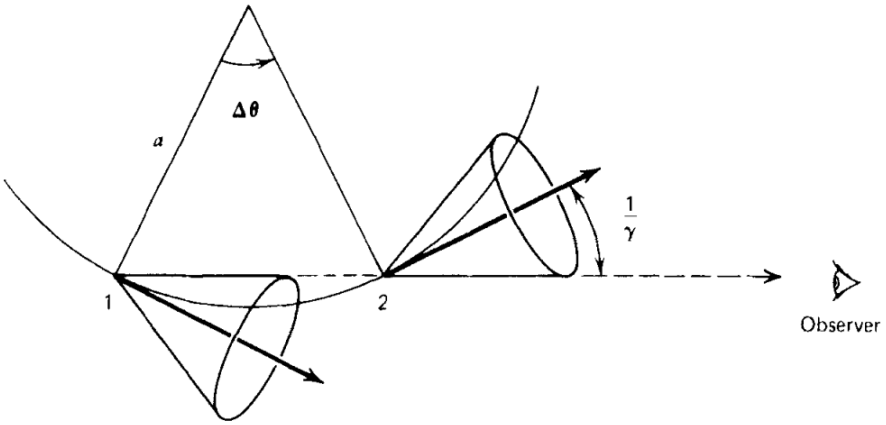

Figure 2.2: Emission cones at various points of an accelerated particle's trajectory (Rybicki & Lightman, 1979)

Characteristic Frequency

The relativistic gyrofrequency (cyclotron frequency) is

$$\omega_B = \frac{eB}{\gamma m_e c}, \tag{2.38}$$

but due to relativistic effects and the broad angular distribution of emission, the power is spread over a spectrum that peaks at the characteristic synchrotron frequency:

$$\omega_c = \frac{3}{2}\gamma^2 \omega_B \sin\alpha = \frac{3}{2}\gamma^2 \frac{eB}{m_e c}\sin\alpha. \tag{2.39}$$

Rybicki and Lightman provide a detailed derivation of this expression of characteristic frequency. I skip the details of derivation as they don't add much to the discussion on the temporal evolution of afterglows.

Spectrum

To get the total power, we will have to take the Fourier transform of the magnetic field seen by the observer.

$$P = \frac{2q^2}{3c^3}\gamma^2 \frac{q^2 B(\omega)^2}{m^2}\beta_\perp^2 \tag{2.40}$$

Rybicki gives a qualitative discussion on what $B(\omega)$ will approximately depend.

Using the expression for Power derived in the time domain, The total power emitted per unit frequency by the electron is given by:

$$P(\omega) = \frac{\sqrt{3}e^3 B\sin\alpha}{2\pi m_e c^2} F\left(\frac{\omega}{\omega_c}\right), \tag{2.41}$$

where the function $F(x)$ is defined as:

$$F(x) = x\int_x^\infty K_{5/3}(z)\,dz, \tag{2.42}$$

with $K_{5/3}$ being the modified Bessel function of the second kind.

The function $F(x)$ encodes the shape of the synchrotron spectrum. It peaks at $x \approx 0.29$ and falls off exponentially for $x \gg 1$, while for $x \ll 1$ it behaves as $F(x) \propto x^{1/3}$. This leads to a broad spectrum with a characteristic power-law form at low frequencies.

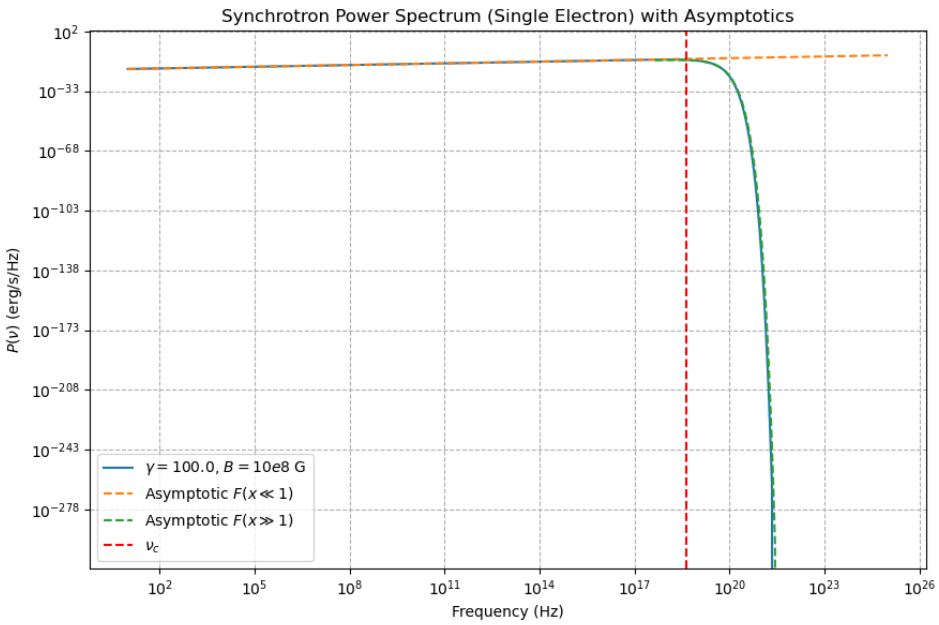

Figure 2.3: Synchrotron Spectrum of a single electron

3.3 Synchrotron Spectrum from a Population of electrons

The population of electrons in the post-shock plasma can be approximated as a power-law distribution in the frame of the shock. In this case, the number of electrons is given by

$$dN(\gamma) \propto \gamma^{-p} dp, \quad \gamma_m < \gamma < \gamma_M \tag{2.43}$$

where:

- γ_m is the minimum Lorentz factor of the population of electrons. item γ_M is the maximum Lorentz factor of the population of electrons.

Therefore

$$P_{tot}(\omega) \propto \int_{\gamma_m}^{\gamma_M} P(\omega)\gamma^{-p} d\gamma \propto \int_{\gamma_m}^{\gamma_M} F(\omega/\omega_c)\gamma^{-p} d\gamma \tag{2.44}$$

Changing variables to $x \equiv \omega/\omega_c$,

$$P_{tot}(\omega) \propto \omega^{-(p-1)/2} \int_{x_m}^{x_M} F(x)\gamma^{(p-3)/2} dx \tag{2.45}$$

Therefore, between a certain range of frequencies, the total power falls as $P \propto \omega^{-(p-1)/2}$. Below the frequency corresponding to the minimum Lorentz factor, all electrons will show ($P(\omega) \propto w^{1/3}$) rise in their spectrum, hence the total spectrum also rises with a spectral index of 1/3. Above the maximum frequency, all electrons will show exponential decay in their spectra. Hence, the total spectrum also decays exponentially. The peak power decreases for increasing Lorentz factors, simply because there are more electrons for a smaller Lorentz factor.

3.4 Key Synchrotron Frequencies

The *key* frequencies are defined as the characteristic frequencies corresponding to the characteristic Lorentz factors. They are the minimum energy Lorentz factor and the cooling Lorentz factor. We will derive the scaling relations for these Lorentz factors and their corresponding characteristic frequencies.

Minimum Energy Lorentz Factor

The minimum energy Lorentz factor corresponds to the Lorentz factor of the highest number of electrons. The minimum Lorentz factor of electrons in post-shock plasma is expected to be of the order of the Lorentz factor of the shock itself. Because electrons accelerate along with shock, they will experience *fermi acceleration* due to the presence of the magnetic field, increasing the Lorentz factor of electrons further. Therefore, the minimum Lorentz factor of electrons is of the order of the Lorentz Factor of the shock, while a population of electrons is accelerated to higher Lorentz factors due to fermi acceleration.

Therefore

$$\gamma_m \propto \Gamma \tag{2.46}$$

The characteristic frequency corresponding to the Lorentz factor is proportional to

$$\nu_m \propto \gamma_m^2 B \tag{2.47}$$

However, the observer will see the frequency boosted by a factor of Γ as we had calculated the spectrum of the population in the frame of the shock. Therefore,

$$\nu_m \propto \Gamma \gamma_m^2 B \propto \Gamma^3 B \tag{2.48}$$

Cooling Frequency

The cooling Lorentz factor can defined using a comoving time scale t' at which electrons with this Lorentz factor lose energy significantly. Simply put, electrons above this Lorentz factor, lose energy very rapidly. This should be clear from our discussion of power emitted in the time domain, where the radiated power is directly proportional to the square of the Lorentz factor.

$$t_{dyn} = \frac{\gamma_c m_e c^2}{\frac{2q^2}{3c^3}\gamma^2 \frac{q^2 B^2}{m^2}\beta_\perp^2} \tag{2.49}$$

Now, t' is defined in the shock frame. It related to the observer frame by simple time dilation formula as follows

$$t_{dyn} = \Gamma t_{obs} \tag{2.50}$$

Combining the above two equations, we can derive the following proportionality relation

$$\gamma_c \propto \Gamma^{-1} t^{-1} B^{-2} \tag{2.51}$$

The characteristic frequency corresponding to γ_c is called cooling frequency and it is proportional to

$$\nu_c \propto \Gamma \gamma_c^2 B \propto \Gamma^{-1} t^{-2} B^{-3} \tag{2.52}$$

3.5 Spectrum from a Population of electrons with continuous injection of electrons

In Gamma-ray bursts, during the propagation of the shock, new energetic particles continuously move across the shock front. Therefore, the synchrotron spectrum obtained in the case of GRBs has to be derived, taking this effect into account. This section refers to (Zhang, 2018).

The distribution and time evolution of particles for an open system of particles is given by the Flokker-Planck equation. We won't go into details of this equation. We will focus on the spectral index which we can derive from the resultant equation. In the GRB, the equation takes the following form:

$$\frac{\partial N(\gamma,t)}{\partial t} = -\frac{\partial\left[\dot{\gamma}N(\gamma,t)\right]}{\partial\gamma} + Q(\gamma,t) \tag{2.53}$$

Let's first understand the meaning and form of each term in the above expression.

- $Q(\gamma,t)$ is the injection term. We will assume that the injection term carries the power-law form as well.

$$Q(\gamma,t) \propto \left[\frac{\gamma}{\gamma_m}\right]^{-p}, \quad \gamma_m < \gamma < \gamma_M \tag{2.54}$$

- $N(\gamma,t)$ is the number of particles within the energy interval $(\gamma, \gamma+d\gamma)$ at a particular time t.

The above equation needs to be solved numerically. But we being devoted astrophysicists, will estimate the resultant power-law index of $N(\gamma,t)$ by taking some order-of-magnitude estimates. The left-hand side of the equation is of the order $\sim N/t$. Assuming, electrons only lose energy by synchrotron radiation, $\dot{\gamma}$ is of the order of $-\gamma/t_{dyn}$, since γ reduces significantly over the dynamical timescale of cooling derived earlier. Hence, the first term on the right hand side is of the order $\sim N/t_{dyn}$. Now, we calculate the power law index of the distribution of electrons in different spectral regimes using order of magnitude estimates.

- $\gamma_m < \gamma < \gamma_c < \gamma_M$: As $\gamma < \gamma_c$, the time scaling of cooling will be very large $(t_{dyn} \gg t)$,i.e. electrons cool very slowly. Hence, the first term of RHS can be neglected. Therefore $N(\gamma,t) \propto \int Q(\gamma,t)dt \propto \gamma^{-p}$.

- $\gamma_m < \gamma_c < \gamma < \gamma_M$: Since $\gamma > \gamma_c$, the electron cools rapidly over the dynamical timescale $(t_{dyn} \ll t)$. Therefore, in this case the first term of the RHS dominates the term on LHS. Therefore $N/t_{dyn} \sim Q$, which gives $N \propto Qt_{dyn} \propto \gamma^{-(p+1)}$

Therefore, we have a very important result. The population of electrons decreases rapidly above the cooling Lorentz Factor. Performing the same analysis as in Section 3.3 of chapter 2, we derive the following spectral index for flux density due to synchrotron radiation in Gamma-ray bursts

$$F_\nu \propto \begin{cases} \nu^{1/3}, & \nu < \nu_m < \nu_c < \nu_M \\ \nu^{-(p-1)/2}, & \nu_m < \nu < \nu_c < \nu_M \\ \nu^{-p/2}, & \nu_m < \nu_c < \nu < \nu_M \\ e^{-\nu/\nu_M}, & \nu_m < \nu_c < \nu_M < \nu \end{cases} \tag{2.55}$$

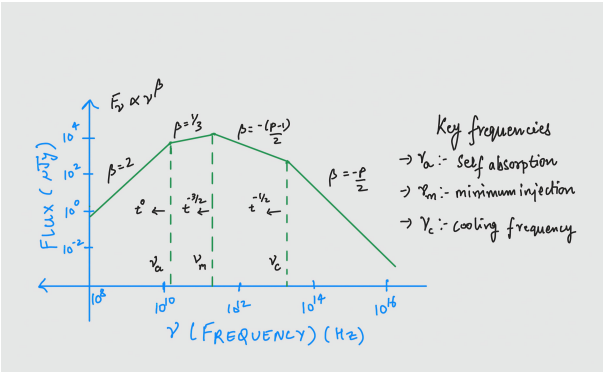

Figure 2.4: Depiction of Synchrotron Spectrum from a GRB Afterglow

The spectrum is depicted in the figure 2.5.

This wraps up our discussion on Synchrotron Radiation. Now we move to the last section of this chapter, the timescales in different frames of reference of the problem. This section refers to chapter 3 of Zhang (2018).

4 Timescales in different frames of reference

There are three important frames of reference in our problem.

- Frame I: The rest frame of the central engine
- Frame II: The rest frame of relativistic ejecta
- Frame III: The rest from of the observer

Within the three frames mentioned, there are two time-scales that concern us

- The relativistic ejecta emission time measured in Frame I (t_e)
- The observation time t_{obs} measured in Frame III

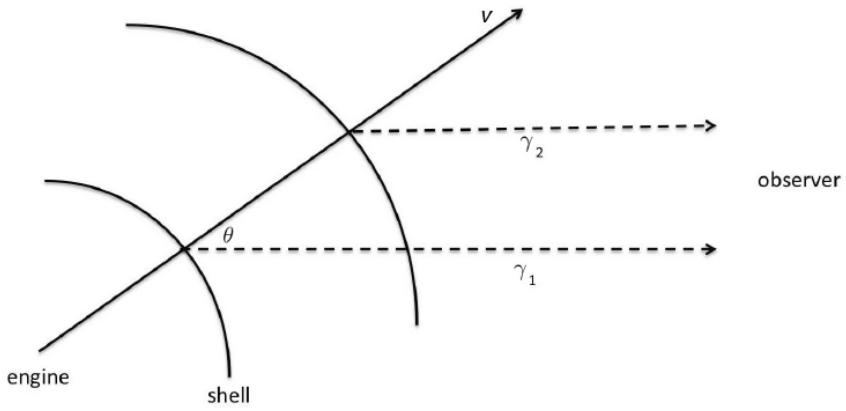

Figure 2.5: Geometry of central engine, ejecta and the observer

I refer to Figure 2.6 to derive the relationship between t_e and t_{obs}. Let $t_{e,1}$ and $t_{e,2}$ be the times at which a light signal starts moving towards the observer. Let $t_{obs,1}$ and

$t_{obs,2}$be the times at which the observer receives the signal 1 and 2 respectively. In the above figure, the first signal is sent out from the location where the v-axis intercepts the inner shell and the second signal is sent out from the location where the v-axis intercepts the outer shell.

Geometrically, these two time intervals can be related through the length of the paths travelled by the signals:

$$c(t_{obs,1} - t_{e,1}) = c(t_{e,2} - t_{e,1})cos(\theta) + c(t_{obs,2} - t_{e,2}) \tag{2.56}$$

This gives

$$\Delta t_{obs} = \Delta t_e(1 - \beta cos(\theta)) \tag{2.57}$$

In the ultra-relativistic limit ($\gamma \gg 1$ and $\theta \simeq 0$), we get

$$\Delta t_{obs} = \frac{\Delta t_e}{2\gamma^2} \tag{2.58}$$

This also a very crucial relation relating the emission time scale in the frame of the central engine to the time frame of the observer.

This ends our chapter on theoretical foundations. We can now move to derive the relations governing the temporal evolution of afterglows.

3 Temporal Evolution of Afterglows

In this chapter, we will derive the temporal evolution of afterglows in three different scenarios

- Constant density surrounding medium (ISM)
- Medium with a density stratification (Wind Medium)
- An interval of dominant stable continuous energy injection by the central engine
- Lastly, we will also study the effects of emission being in a cone on afterglow fading

This chapter is based on chapter 8 of Zhang (2018).

1 Temporal Evolution of Bulk Lorentz Factor of the jet

The jet's Lorentz Factor (Γ) plays a crucial role in determining how fast the afterglow fades. The Lorentz Factor also plays a crucial role in the temporal evolution of synchrotron key frequencies, as we saw in the previous chapter. In this section I will derive the evolution of the Bulk Lorentz factor in the three scenarios described above

1.1 Evolution of Bulk Lorentz Factor in a constant density ISM

We first consider the case of a constant-density ISM. Referring to the formula of the energy density of the shocked medium derived in section 1 of chapter 2, we can write the total Energy of the shocked medium as

$$E \sim enm_p c^2 \Gamma^2 = \text{constant} \tag{3.1}$$

where the volume swept by the shock is $\frac{4\pi}{3} r^3$.

We therefore get $\Gamma^2 r^3 = \text{constant}$.

We also derived the relation between the time evolution of shock in the frame of the central engine and the observer time. In the central engine frame, the evolution time scale of the shock is simply r/c. Therefore

$$t_{obs} = \frac{r}{2\Gamma^2 c} \propto r\Gamma^{-2} \tag{3.2}$$

Combining the above two equations, we get

$$\Gamma \propto r^{-3/2} \propto t_{\text{obs}^{-3/8}} \tag{3.3}$$

This is how the Bulk Lorentz factor evolves in a constant density ISM.

1.2 Evolution of Bulk Lorentz Factor in an ISM with stratified density profile

Here, we can introduce a general density profile parameterized by k.

$$n = n_0 \left(\frac{r}{r_0}\right)^{-k} \tag{3.4}$$

Therefore, the total energy will then be written as

$$E \sim \int 4\pi r^2 n_0 \left(\frac{r}{r_0}\right)^{-k} m_p c^2 \Gamma^2 dr = \text{constant} \tag{3.5}$$

Integrating the above equation, we get $r^{3-k}\Gamma^2 = \text{constant}$. Carrying out the same analysis we did for constant density ISM, we get

$$\Gamma \propto r^{(3-k)/2} \propto t^{(k-3)/(8-2k)} \tag{3.6}$$

For different progenitor stars, we can expect different values of k depending upon the nature of their stellar winds. The most commonly accepted value in the case of GRB Progenitors is $k = 2$, which is the value for a Wolf-Rayet Star. For $k = 2$, the above relations are

$$\Gamma \propto r^{-1/2} \propto t^{-1/4} \tag{3.7}$$

This equation describes the temporal evolution of Bulk Lorentz factor in case of a *Wind* medium.

1.3 Evolution of Bulk Lorentz Factor with dominant energy injection from the Central Engine

In general, we would expect the shock energy to decrease with time as the shock decelerates with its interaction with the external medium. That is the case; we observe the fluxes decrease to decrease with time, and the afterglow fades. However, it might be that the central engine, after the initial burst, becomes active again and starts sourcing the shock again. We will discuss the case where the energy injected by the central engine at a time after the initial burst, starts dominating the shock, i.e. the total energy of the shock at that time is dominated by the injected energy and not the initial energy.

Let the central engine injection be formulated by

$$L(t) = L_0 \left(\frac{t}{t_0}\right)^{-q} \tag{3.8}$$

Then

$$E_{\text{inj}} = \int_{t_0}^{t} L(t)\, dt = \begin{cases} \frac{L_0 t_0^q}{1-q}\left(t^{1-q} - t_0^{1-q}\right) \simeq \frac{L_0 t_0^q}{1-q} t^{1-q}, & \text{for } t \gg t_0, \quad q < 1, \\ L_0 t_0 \ln\left(\frac{t}{t_0}\right), & q = 1, \\ \frac{L_0 t_0^q}{q-1}\left(t_0^{1-q} - t^{1-q}\right) \simeq \frac{L_0 t_0}{q-1}, & \text{for } t \gg t_0, \quad q > 1, \end{cases} \tag{3.9}$$

It is quite clear from the above equations that only when $q < 1$, that the blastwave has a significant contribution from the energy injection by the central engine. In the case

of $q > 1$, the central engine activity, even if present, will have negligible contribution to the shock energy and would be very hard to observe. Therefore, we only discuss the case with $q > 1$.

For $q > 1$

$$E_{\rm tot} \sim E_{\rm inj} \propto t^{1-q} \tag{3.10}$$

For constant-density ISM, we have

$$\Gamma^2 r^3 \propto t^{1-q} \tag{3.11}$$

Introducing the scaling with the *observer time* ($t_{\rm obs} \propto r\Gamma^{-2}$), we get

$$\Gamma^2 r^3 \propto r^{1-q}\Gamma^{2(q-1)} \tag{3.12}$$

Solving for Γ we get

$$\Gamma \propto r^{(2+q)/(4-2q)} \propto t^{-(2+q)/8} \tag{3.13}$$

For the stratified density case, we have

$$\Gamma^2 r^{(3-k)/2} \propto t^{(1-q)} \tag{3.14}$$

Introducing observer time dependence, we get

$$\Gamma^2 r^{(3-k)/2} \propto r^{1-q}\Gamma^{2(q-1)} \tag{3.15}$$

Isolating Γ gives

$$\Gamma \propto t^{(k-q-2)/(8-2k)} \propto r^{(2+q-k)/(2q-4)} \tag{3.16}$$

Plugging in $k = 2$ for Wolf-Rayet wind, we get

$$\Gamma \propto r^{q/(2q-4)} \propto t^{-q/4} \tag{3.17}$$

2 Temporal Evolution of Afterglow Flux in constant density ISM

Now that we have figured out temporal evolution of the Bulk Lorentz factor, we can derive the temporal evolution of afterglow flux. We will combine the scaling of key synchrotron frequencies with the synchrotron power spectrum and derive the time evolution of flux.

Before that, we should figure out the dependency of the magnetic field, as it plays a crucial role in determining the evolution of the Bulk Lorentz Factor.

2.1 Evolution of the Magnetic Field

Like mentioned above, in order to calculate synchrotron frequencies, we need to calculate the strength of the comoving Magnetic field. Assuming a fraction ϵ_B of the energy density of the post-density shock medium does into the magnetic field, the magnetic field energy density can be described as

$$B^2 \sim \Gamma^2 \epsilon_B n m_p c^2 \implies B \propto \Gamma \tag{3.18}$$

Moreover, from the power spectrum of a single electron, we have

$$P \propto B \tag{3.19}$$

However, this is the power that is being emitted in the frame of the shock. Therefore, for the observer, it will be boosted by the factor of Γ. Therefore

$$P \propto \Gamma B \tag{3.20}$$

Note that the relation for the power spectrum of a single electron holds for wind media as well, as in deriving it, we made no assumption about the density profile of the external medium.

2.2 Evolution of key synchrotron frequencies

In this subsection, we will derive the temporal evolution of the key synchrotron frequencies (ν_m, ν_c) and also $F_{\nu,\max}$ to calculate the final synchrotron spectrum from a population of electrons in GRB afterglows. Kindly refer to the section on synchrotron radiation for any problems faced in going through the proportionality relations here, as I won't re-derive those.

$$\nu_m \propto \Gamma \gamma_m^2 B \propto \Gamma^4 \propto t^{-3/2} \tag{3.21}$$

$$\nu_c \propto \Gamma \gamma_c^2 B \propto \Gamma^{-1} t^{-2} B^{-3} \propto t^{-1/2} \tag{3.22}$$

$$F_{\nu,\max} \propto N_{\rm tot} P_{\nu,\max} \propto r^3 B \Gamma \propto t^0 \tag{3.23}$$

Here, we have a very important result, that $F_{\nu,\max}$ is a constant in time for constant density ISM!

Putting the above relations in the synchrotron spectrum

$$F_\nu \propto \begin{cases} \nu^{1/3}, & \nu < \nu_m < \nu_c \\ \nu^{-(p-1)/2}, & \nu_m < \nu < \nu_c \\ \nu^{-p/2}, & \nu_m < \nu_c < \nu \end{cases} \tag{3.24}$$

we get

$$F_\nu \propto \begin{cases} t^{1/2}, & \nu < \nu_m < \nu_c \\ t^{-3(p-1)/4}, & \nu_m < \nu < \nu_c \\ t^{(-3p+2)/4}, & \nu < \nu_c < \nu \end{cases} \tag{3.25}$$

The figure below is a simulation of afterglow flux in constant density ISM.

3 Temporal Evolution of Afterglow flux in Wind Medium

In this section, I will derive the temporal evolution of afterglow flux in Wind Medium. We will solely focus on the case $k = 2$, i.e. wind from the Wolf-Rayet stars. This is because, in the analysis of GRB afterglows, we generally do not fit k as a parameter. Hence, I will derive the relations for afterglow flux, making the most widely accepted assumption for the value of k, i.e. $k = 2$.

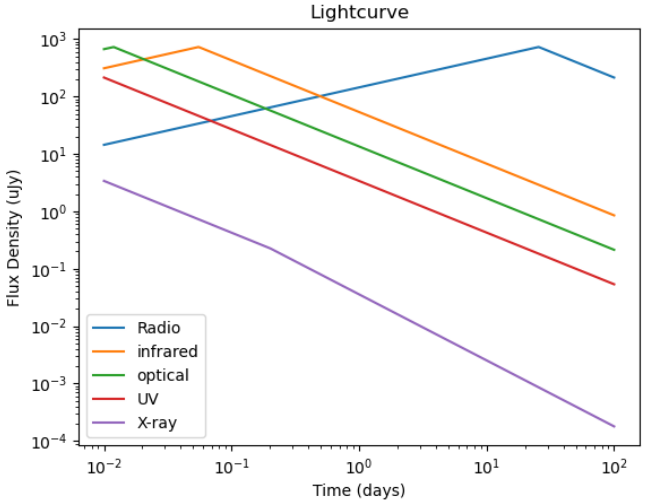

Figure 3.1: Afterglow lightcurve in constant density ISM. We can observe the ν_m breaks in Radio, infrared and optical, with cooling break ν_c visible in the X-ray regime.

3.1 Evolution of the Magnetic Field

Following our own footsteps from the constant density case, we get

$$B^2 \propto \Gamma^2 r^- 2 \propto \Gamma^6 \tag{3.26}$$

In the case of wind media, we observe a very strong dependence of the comoving magnetic field strength on the Bulk Lorentz factor compared to the constant density ISM case.

3.2 Evolution of key synchrotron frequencies

The evolution of key synchrotron frequencies and $F_{\nu,\max}$ in the case of stellar wind can be derived following the steps we did in the ISM case. The relations are

$$\nu_m \propto \Gamma \gamma_m^2 B \propto \Gamma^6 \propto t^{-3/2} \tag{3.27}$$

$$\nu_c \propto \Gamma \gamma_c B \propto \Gamma^{-10} t^2 \propto t^{1/2} \tag{3.28}$$

$$F_{\nu,\max} \propto r \Gamma B \propto \Gamma^2 \propto t^{-1/2} \tag{3.29}$$

Again, we make some interesting observations here. $F_{\nu,\max}$ decreases with time in the case of wind medium compares to being constant in time in the constant density ISM case. The cooling frequency increases with time! This makes it quite difficult to observe a cooling break in wind medium afterglows, as the cooling frequency might be quite high to begin with. And as we shall see, in wind media, the afterglow actually fades at a slower rate post the cooling break.

Putting the above relations in the synchrotron spectrum

$$F_\nu \propto \begin{cases} \nu^{1/3}, & \nu < \nu_m < \nu_c \\ \nu^{-(p-1)/2}, & \nu_m < \nu < \nu_c \\ \nu^{-p/2}, & \nu_m < \nu_c < \nu \end{cases} \tag{3.30}$$

we get

$$F_\nu \propto \begin{cases} t^0, & \nu < \nu_m < \nu_c \\ t^{(-3p+1)/4}, & \nu_m < \nu < \nu_c \\ t^{(-3p+2)/4}, & \nu < \nu_c < \nu \end{cases} \tag{3.31}$$

Here, we make yet another important observation that can help distinguish between constant-density ISM and Wind afterglows. In case of wind medium, the flux is constant in time before the ν_m break! This can be observed in late radio band data and is key signature of wind medium afterglows.

The figure below simulates the afterglow flux in a wind medium.

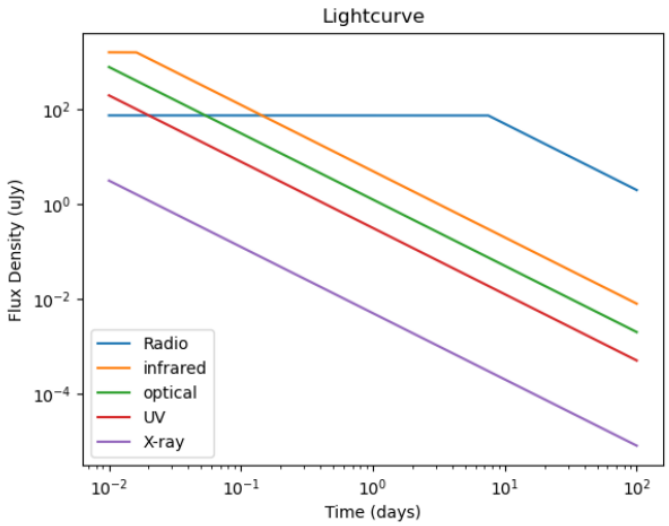

Figure 3.2: Simulation of afterglow light curve in wind medium. We can observe the flux in the radio band being constant in time before the passing of ν_m

4 Jet Effects

The ejecta from the explosion in GRBs is believed to be collimated. The effect of this collimation is observed in fading of afterglow fluxes through the phenomenon of "jet break". It is a break in afterglow fading slopes that theoretically occurs at the same time across all wavelengths, because the reason for the effect is geometrical. In the following subsections, I will derive the amount of change in slope we expect due to this effect in different media (Zhang, 2018).

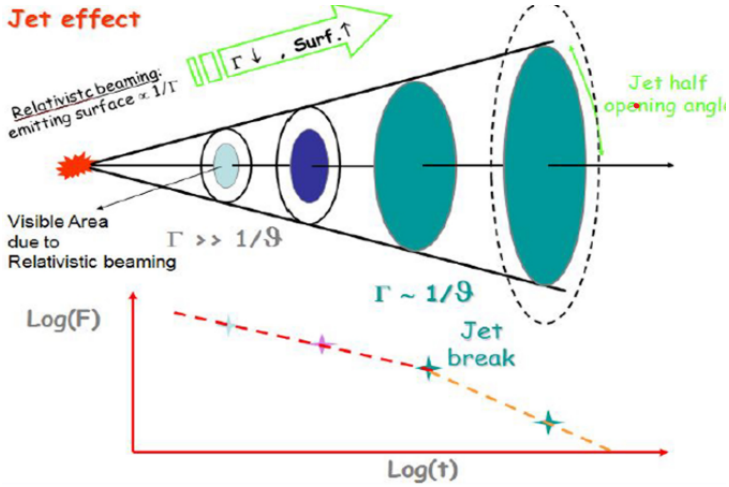

Figure 3.3: Schematic showing the break in light curve fading due to beamed emission of the jet. (Dainotti, 2019)

Refer to Figure 3.3 for visual guidance while following the math in the following sections.

4.1 Jet Break in ISM & Wind

Consider a conical jet with an opening angle of θ_{jet}. Before the break time, we have $\Gamma^{-1} \ll \theta_{\text{jet}}$, and observer has no knowledge about the beaming of the jet, because the observed emission dominantly comes within the $1/\Gamma$ cone within the jet cone.

Post the jet break ($\Gamma^{-1} \gg \theta_{\text{jet}}$), the observed flux starts to decay faster, as the observer starts noticing the effect of lack of material to produce radiation outside the jet cone. Note that there is no change in the dynamics of the jet itself. It is purely a geometric effect.

The key modification occurs in the scaling relation of $F_{\nu,\max}$. The scaling relation of $F_{\nu,\max}$ gets a correction factor of the ratio between the jet's solid angle and the emission cone's solid angle. The correction factor can be evaluated to be $\frac{\theta_{\text{jet}}^2}{(1/\Gamma)^2}$ by taking the small-angle limit in the expression for solid angle and half angle of the cone.

ISM

In the ISM case we have from equation 3.23:

$$F_{\nu,\max} \propto r^3 B' \Gamma \frac{\theta_j^2}{(1/\Gamma)^2} \propto r^3 B' \Gamma^3 \propto t^{-3/4}. \tag{3.32}$$

Therefore, we have a steepening from t^0 to $t^{-3/4}$. Therefore, the light curve in all regimes steepens by a factor of 0.75 in the ISM case.

Wind

Referring to equation 3.29, we have

$$F_{\nu,\max} \propto rB'\Gamma \frac{\theta_j^2}{(1/\Gamma)^2} \propto rB'\Gamma^3 \propto t^{-1}, \tag{3.33}$$

Therefore, we have a steepening from $t^{-1/2}$ to t^{-1}. Therefore, the light curve in all regimes steepens by a factor of 0.5 in the wind case.

Rhoads (1999) studied additional effects of lateral expansion of the jet on observed fading of the light curve. Rhoads (1999) found that the lateral expansion of jets results in even steeper decays of afterglow light curves.

4 Modelling of GRB Afterglows

Having developed a detailed theoretical understanding of GRB afterglows, I now turn to an analysis of observational data. We can fit the light curves of GRBs using semi-analytic models and Bayesian inference techniques to constrain the physical parameters that govern the evolution of the burst. For all the analyses, I use the Bayesian nested sampling algorithm provided by the dynesty package to fit light curves using the semi-analytical models presented in Gao et al. (2013).

1 GRB230204B

I employed multiband data for GRB230204B across X-ray, optical and radio frequencies. The model I use to do the fits is the *adiabatic expansion without energy injection in wind media* from (Gao et al., 2013). I have written down the equations governing the model below for completion.

1.1 Model

$$\nu_m = 2.2 \times 10^{10}\,\mathrm{Hz}\,\hat{z}^{1/2}\left(\frac{G(p)}{G(2.3)}\right)E_{52}^{1/2}\epsilon_{e,-1}^{2}\epsilon_{B,-2}^{1/2}t_5^{-3/2}, \tag{4.1}$$

$$\nu_c = 1.8 \times 10^{18}\,\mathrm{Hz}\,\hat{z}^{-3/2}E_{52}^{1/2}A_{*,-1}^{-2}\epsilon_{B,-2}^{-3/2}t_5^{1/2}, \tag{4.2}$$

$$F_{\nu,\max} = 1.5 \times 10^{3}\,\mu\mathrm{Jy}\,\hat{z}^{3/2}E_{52}^{1/2}A_{*,-1}\epsilon_{B,-2}^{1/2}D_{28}^{-2}t_5^{1/2}. \tag{4.3}$$

where

- $\hat{z} = (1+z)/2$ is the redshift correction factor
- $$G(p) = \left(\frac{p-2}{p-1}\right)^2 \tag{4.4}$$
- $E_{K,52}$ is the isotropic equivalent kinetic energy of the jet in units of 10^{52} ergs
- $\epsilon_{e,-1}$ is the fraction of energy in electrons in units of 0.1
- $\epsilon_{B,-2}$ is the fraction of energy in the magnetic field in units of 0.01
- t_5 is the observer time in the units of 10^5 seconds
- $A_{*,-1}$ is a parameter related to mass-loss rate through stellar wind and wind speed in units of 0.1
- D_{28} is the luminosity distance in units of 10^{28} centimeters

1.2 Fits :- Light Curves and Corner Plots

The parameters for the model were sampled using dynesty. I cross-validate the posterior distributions produced by dynesty using the affine-invariant sampler emcee as well. The resultant fits from both samplers are provided below.

Dynesty

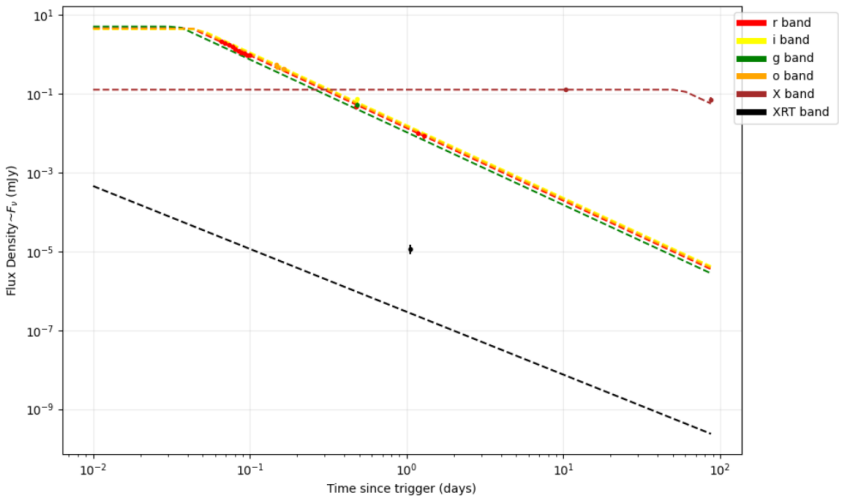

Figure 4.1: Multiband afterglow light curve of GRB230204B. The data points represent the observed fluxes across different frequencies, while the solid lines show the best-fit model predictions from dynesty

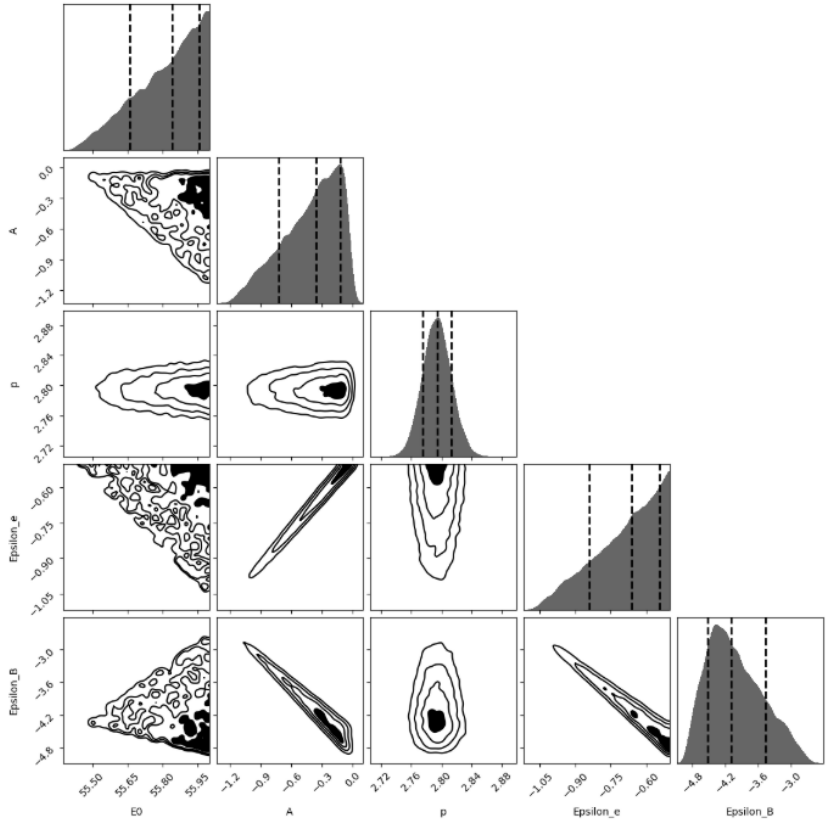

Figure 4.2: Corner Plots showing the marginalized and joint posterior distributions for the fitted parameters from the dynesty sampler

Emcee

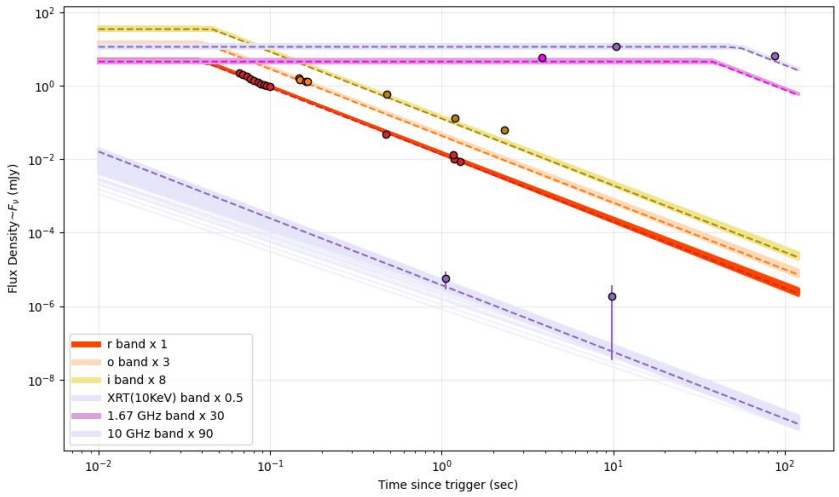

Figure 4.3: Multiband afterglow light curve of GRB230204B. The data points represent the observed fluxes across different frequencies, while the solid lines show the best-fit model predictions from emcee. Credits :- Vishwajeet (STAR Lab)

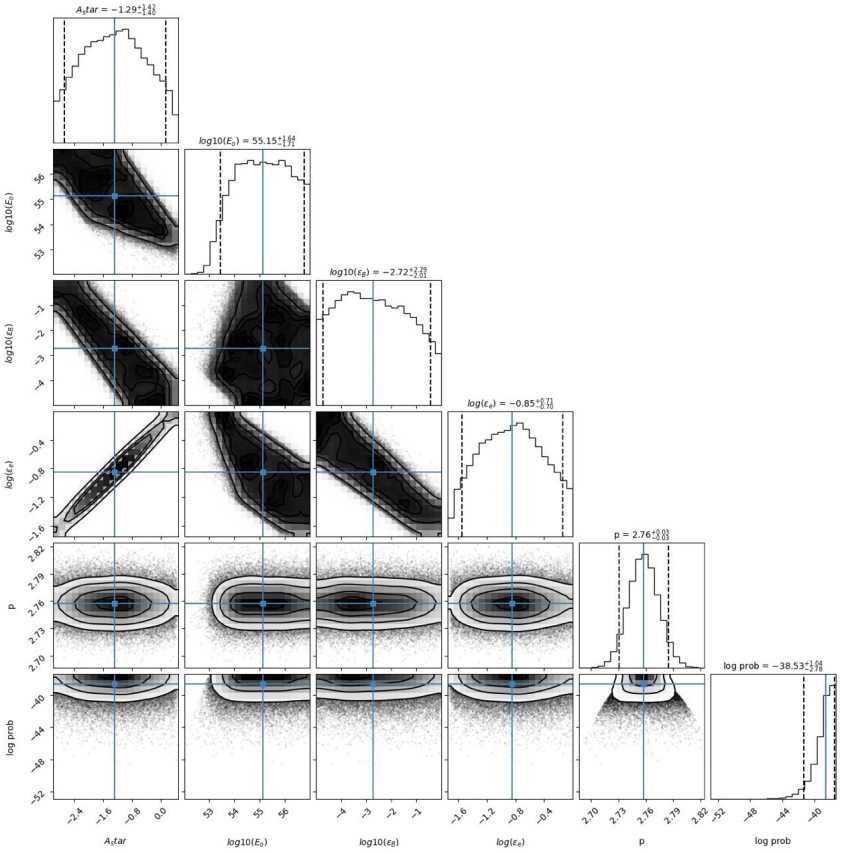

Figure 4.4: Corner Plots showing the marginalized and joint posterior distributions for the fitted parameters from the emcee sampler. Credits :- Vishwajeet (STAR Lab)

Comparison of best-fit parameters

Table 4.1: Best-fit parameters and 1σ standard deviations from `emcee` and `dynesty` samplers.

Parameter	Best-fit (emcee)	errors (emcee)	Best-fit (dynesty)	Std. Dev. (dynesty)
$\log(E_{\rm K,iso})$	55.15	1.4	55.81	0.13
$\log(\epsilon_e)$	-0.85	0.7	-0.68	0.13
$\log(\epsilon_B)$	-2.72	2.2	-4.01	0.5
$\log(A_*)$	-1.29	1.42	-0.41	0.27
p	2.76	0.04	2.79	0.02

1.3 Discussion

One of the key successes of the model is explaining the constant flux signature in late radio data, which was theoretically predicted by equation 3.31 for the $\nu < \nu_m < \nu_c$ regime. The best-fit parameter values obtained by both **dynesty** and **emcee** agree with each other within the error bars. It is a good sign that the inferred values of p agree with each other, since we saw in section 3 how the slope of afterglow decay is directly governed by the value of electron population index (p). Additionally, the value of $E_{\rm K,iso}$ suggests a highly energetic event. Vishwajeet performed the analysis of prompt emission and found the energy released in prompt emission to be around $E_{\gamma,\rm iso} \sim 2.2 \times 10^{54}$. This suggests a GRB with low efficiency. Low efficiency means that the total energy released in prompt emission is much less than the energy in the afterglow emission, which agrees with the fireball model(Piran, 1999).

5 Future Works and Acknowledgements

The current work focuses on fixing the script for analysing Gamma-Ray Bursts (GRBS) in an ambient medium characterised by a constant density interstellar medium (ISM). We successfully conducted the wind case analysis; however, we are unable to extract physically meaningful results for the ISM case. The GRB being studied in the ISM context is GRB210204A.

The project began with two main aims. I have made significant progress on the first aim, which is to build a theoretical understanding of the fundamental principles and to theoretically derive the fading rates of GRB afterglows. The second aim is to conduct a bulk analysis of GRBs in the GROWTH-India catalogue. I am collaborating with Vishwajeet on this second goal. Our objective is to categorise the GRBs in the GROWTH-India catalogue based on whether the ambient medium is ISM or Wind. Additionally, we will determine if any of these GRBs exhibit signatures of reverse shocks in early-time data, and we will analyse them accordingly.

Bibliography

Berger, E. 2014, Annual Review of Astronomy and Astrophysics, 52, 43

Dainotti, M. 2019, in Gamma-ray Burst Correlations, 2053-2563 (IOP Publishing), 2–1 to 2–23

Fishman, G. J., & Meegan, C. A. 1995, Annual Review of Astronomy and Astrophysics, 33, 415

Gao, H., Lei, W.-H., Zou, Y.-C., Wu, X.-F., & Zhang, B. 2013, New Astronomy Reviews, 57, 141

Gehrels, N., Ramirez-Ruiz, E., & Fox, D. B. 2009, Annual Review of Astronomy and Astrophysics, 47, 567

Klebesadel, R. W., Strong, I. B., & Olson, R. A. 1973, The Astrophysical Journal, 182, L85

Kouveliotou, C., et al. 1993, The Astrophysical Journal, 413, L101

Kumar, P., & Zhang, B. 2015, Physics Reports, 561, 1

Landau, L. D., & Lifshitz, E. M. 1987, Fluid Mechanics, Second Edition: Volume 6 (Course of Theoretical Physics), 2nd edn., Course of theoretical physics / by L. D. Landau and E. M. Lifshitz, Vol. 6 (Butterworth-Heinemann)

Meszaros, P. 2006, Reports on Progress in Physics, 69, 2259

Metzger, M. R., et al. 1997, Nature, 387, 878

Nakar, E. 2007, Physics Reports, 442, 166

Padmanabhan, T. 2000, Theoretical Astrophysics - Volume 1, Astrophysical Processes, by T. Padmanabhan, pp. 622. Cambridge University Press, December 2000. ISBN-10: 0521562406. ISBN-13: 9780521562409. LCCN: QB461 .P33 2000, doi:10.2277/0521562406

Piran, T. 1999, Physics Reports, 314, 575

—. 2004, Reviews of Modern Physics, 76, 1143

Rhoads, J. E. 1999, , 525, 737

Rybicki, G. B., & Lightman, A. P. 1979, Radiative Processes in Astrophysics (New York: Wiley)

Sari, R., Piran, T., & Narayan, R. 1998, The Astrophysical Journal, 497, L17

Thorne, K. S., & Blandford, R. D. 2018, Modern classical physics (New Jersey:: Princeton University Press,)

van Paradijs, J., et al. 1997, Nature, 386, 686

Woosley, S. E., & Bloom, J. S. 2006, Annual Review of Astronomy and Astrophysics, 44, 507

Zangwill, A. 2012, Modern Electrodynamics (Cambridge University Press)

Zhang, B. 2018, The Physics of Gamma-Ray Bursts (Cambridge, UK: Cambridge University Press), provided by the SAO/NASA Astrophysics Data System, doi:10.1017/9781139226530